

The Computable Plant: Annual Report, 6/2007-5/2008

Eric Mjolsness, Principal Investigator
Institute for Genomics and Bioinformatics
University of California, Irvine
emj@uci.edu

Elliot Meyerowitz, co-Principal Investigator
California Institute of Technology
meyerow@caltech.edu

Contents

<i>1. Introduction</i>	<i>2</i>
<i>2. Biological Modeling</i>	<i>2</i>
<i>3. Image Analysis</i>	<i>13</i>
<i>4. Mathematical and Software Tools</i>	<i>29</i>
<i>5. Activities and Meetings</i>	<i>31</i>
<i>6. K-12 Outreach</i>	<i>35</i>
<i>7. Research Dissemination</i>	<i>41</i>

1. Introduction

Activities this year fall in the categories of biological modeling, image analysis, mathematical and software tools, meetings, outreach, and dissemination as detailed below. Many papers, images, and software tools are available on the Computable Plant project web site, www.computableplant.org.

2. Biological Modeling

2.1 Computational modeling of the sepal epidermis (Chickarmane and Roeder)

Last year we initiated the expansion of the computable plant project to address the development of lateral organs by focusing on the sepal as an initial model. The sepal is the outermost green leaf-like floral organ. Similar to the leaf and stem, the sepal epidermis contains cells with a wide variety of sizes from giant cells to small cells (Figure 1A-1B). The mechanism through which this pattern of cells with diverse sizes is generated remains unknown. Giant cells enlarge through a specialized cell cycle called endoreduplication in which the cell replicates its DNA, but fails to divide, and consequently becomes enlarged. Similar to the leaf, we have verified that the size of each sepal cell corresponds with its DNA content or ploidy. Once a cell endoreduplicates, it is no longer capable of dividing. We hypothesize that there are a limited number of cell cycles that each cell can apportion between endocycles and mitotic cycles. If a cell starts to endoreduplicate early, all of the subsequent cell cycles are also endocycles and consequently the cell becomes enlarged. On the other hand, if a cell decides to divide early, it remains small. Therefore, we predict that the timing of endoreduplication controls the ultimate cell size.

Over the past year we have used a geometric model to test whether this hypothesis can reproduce the pattern of cell sizes found on the sepal epidermis. Our model was based on several assumptions. First we assumed that all cells grow at the same rate regardless of size to prevent distortions in the sheet of cells. Plant cell walls constrain the cells and prevent them from slipping relative to one another. Therefore, we modeled the overall sepal as an expanding rectangle upon which we superimposed cells that expand with the overall rectangle. Second, we assumed that all cells undergo either the mitotic cell cycle or the endocycle and that both of these cell cycles have the same period. To model the cell cycle, we created a simple protein oscillator in each cell. Third, we assumed that when the cell cycle of a 2C cell reaches a threshold “decision point,” the cell must decide whether to divide or endoreduplicate randomly with a given probability. Fourth, we assumed that once a cell enters endoreduplication it can no longer divide and must undergo another endocycle the next time its cell cycle reaches the decision point. Fifth, we assumed that the total number of endocycles undergone by the most highly endoreduplicated giant cell represents the maximum number of cycles that the tissue undergoes regardless of whether those cycles are mitotic cycles or endocycles. At the time the model was created, we limited the number of cell cycles to 5 because ploidy of giant cells was unknown. Now we find that giant cells are 16C, so next year we will revise the model to limit all cells to 3 cell cycles. Sixth, we assumed that a cell approximately doubles its area in each cell cycle, so we have adjusted the cell cycle time

to correspond with the growth rate. When we satisfy all of the above conditions, the outcome of running this model closely resembles the cell size distribution pattern of the sepal epidermis (Figure 1C).

We have tested our computational model two ways. As will be described below, we used live imaging to record the development of the sepal and have observed that the giant cells enter endoreduplication early while the small cells continue to divide as predicted in our model (see below). Second we have tested our model by changing the probability with which cells endoreduplicate to determine if the simulated sepals match the sepals of plants in which endoreduplication is promoted or inhibited. First, if we increase the probability of endoreduplication, the simulated sepals are largely covered by giant cells similar to the sepals of *ATML1::KRP1* transgenic plants (kindly provided by Dr. Keiko Torii) in which the cell cycle inhibitor *KRP1* is expressed throughout the epidermis (Figure 1G-1I). Conversely, if we decrease the probability of entering endoreduplication early in sepal development, our computational model produces sepals without giant cells (Figure 1F). In a screen for *Arabidopsis* mutants that fail to produce giant cells in the sepal epidermis, we isolated the *loss of giant cells from organs (lgo)* mutant. The sepals of *lgo* mutants are completely covered by small cells (Figure 1D-1E), however, the overall size of the sepals is slightly larger than wild type, showing that the growth of the sepals is not affected. Endoreduplication is not generally affected in the *lgo* mutant, since the highly endoreduplicated hair cells, or trichomes, form normally. Upon positional cloning we found that *LGO* encodes a small putative cell cycle inhibitor in the plant specific *SIAMESE* family. We conclude that cell cycle inhibitors are likely to regulate the timing of endoreduplication and consequently the cell size pattern.

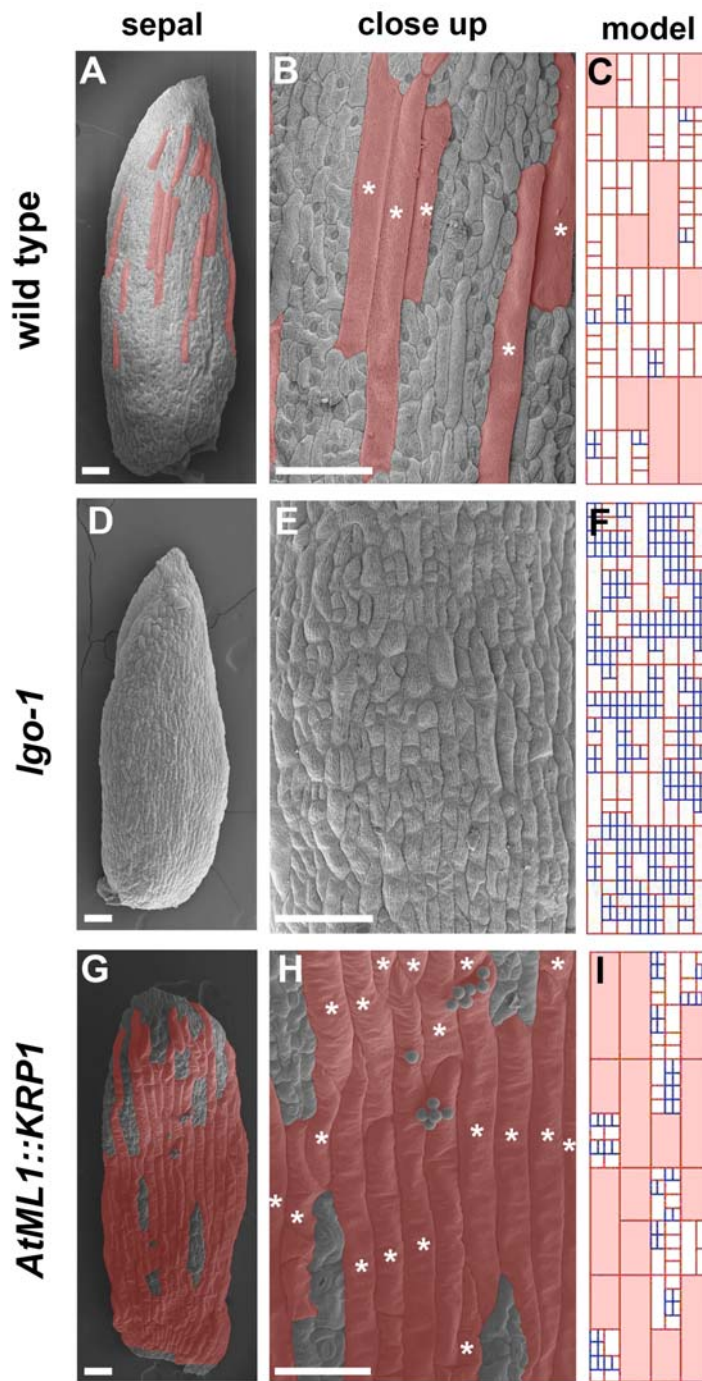


Figure 1: Computational modeling of sepal development

Wild type (A-C) sepals have giant cells (red asterisks) interspersed between smaller cells. The giant cells stretch a third the length of the sepal (A). Note that the giant cells are clustered (B). Our computational model simulates the cell size distribution pattern in the sepals (C).

Igo-1 (D-F) sepals do not contain giant cells (D), although the small cells take a range of sizes (E) as in wild type. Decreasing the probability of entering endoreduplication in the first two cell cycles of the model recapitulates the lack of giant cells phenotype (F).

ATML1p::KRP1 (G-I) sepals are nearly covered with giant cells (G and H). Only islands of small cells remain. Increasing the probability of entering endoreduplication during the first cell cycle in the model recapitulates the *ATML1p::KRP1* phenotype including the islands of small cells (I).

2.2 Cytokinin Perception (Gordon and Chickarmane).

How do plant cells perceive the plant hormone, cytokinin, which is known to be an activator of several biological processes such as cell proliferation, cell senescence, etc. Experiments over the last several years have shown that the underlying biochemical network is essentially composed of a two-component signaling network involving

histidine kinases, and the type A & B Arabidopsis response regulators (ARR's). The network responds to cytokinin by using signaling and gene regulatory interactions which have the ultimate effect of inducing negative feedback of cytokinin activity. Our broad goal is to understand how this network functions, not only as sensitivity of plants to cytokinin, but also ultimately as to how cytokinin gradients can pattern plant development. Our experiments so far suggest that cytokinin induces Wuschel, an important transcription factor which is responsible for sensitizing the plant to cytokinin, and also controlling the number of stem cells in the upper part of the shoot apical meristem zone. There are however two competing hypothesis as to how this induction could occur.

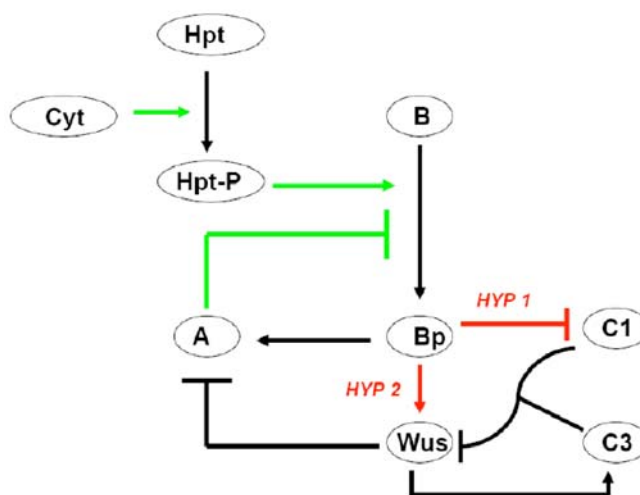


Figure 2: The interaction network between various components of the cytokinin signaling network. The two main hypotheses marked in red suggest that cytokinin induction occurs either through suppression of CLV1, or through direct induction of Wus through type B ARR's. (Hpt-Phospho transfer protein, A, B refer to type A, type B ARR's, C1, C3-CLV1, CLV3)

In Figure 2 is shown the putative network, which suggests that cytokinin could either repress CLV1, which leads to activation of Wus, or activate Wus directly through type B ARR's. As a way to test from among these hypotheses, we have developed a computational model of this network by modeling the protein levels by differential equations. Our model has the advantage of being able to test various hypotheses by successively “pruning” the network connections, i.e without altering any of the network parameters, to generate concentration levels of Wus for hypotheses (1) & (2). Such a method we believe is very useful, as no additional assumptions need to be made. We have simulated the model for the various hypotheses, with High/Low concentration of cytokinin, corresponding to treated/mock treated respectively, in an experiment in which we apply auxin to the shoot apex and measure the concentration of various of the components in the model. Figure 3, displays the fold changes that occur in the simulation, which we can compare to the experimentally obtained changes. The model suggests that the largest change occurs when cytokinin induces Wuschel through type B ARR's. We are currently using confocal microscopy and profiling gene expression to test the specific predictions made by the model.

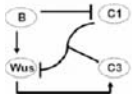
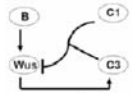
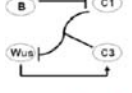
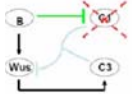
	Mock	Treated	Fold Ch
	0.01	1.32	132
	0.01	0.09	9
	0.01	0.02	2
	0.1	7.23	72

Figure 3. For each of the hypotheses schematized in the leftmost column, we compute the fold changes for mock-treated and cytokinin-treated tissue. The simulations correspond to the steady state level of *Wuschel* for low/high levels of cytokinin, for each of the networks shown. The networks themselves are subsets of the larger network shown in Figure 2, with the appropriate connection set to zero. The fold change for direct activation of *Wus* through type B ARR is the largest.

In trying to understand the functionality of the network, we have developed a much more elaborate model of cytokinin perception, which includes the previous model as a subnetwork. This model which is partly based upon a recent review by Muller & Sheen (Science **318**, 68-69, 2007), is schematically shown in Figure 4.

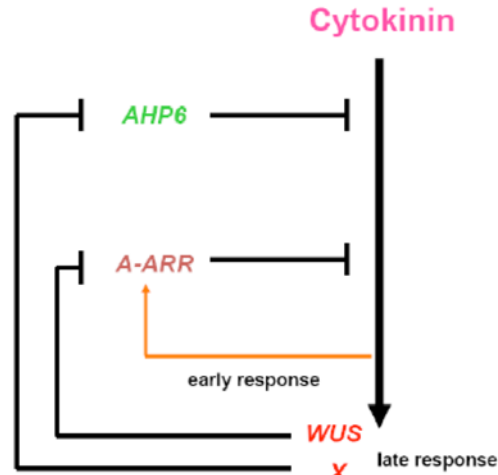


Figure 4: A schematic showing regulatory interactions of the cytokinin perception network showing two (similar in regulatory architecture) nested loops: The outer loop shows AHP6, which reduces the cytokinin signal and is regulated by an X gene, the latter itself is regulated by the incoming cytokinin signal. The inner loop once again contains negative regulation of the signal through type A ARR's which are themselves transcribed by type B ARR's (not shown). The type A ARR's are suppressed by *Wus*, which is hypothesized to be induced by the signal. This leads to two nested positive feedback loops, which gives rise to interesting switch-like behavior.

One of the central questions which we address in this model is which mechanisms can allow the cell to respond to different hormone levels, such that at each input level, a different program is activated for a different threshold, for example, leaf senescence vs vascular differentiation vs shoot initiation, all effects of cytokinin concentration changes.

The computational model of the signaling-genetic circuit suggests that the network functions as a multilevel switch, such that at varied threshold levels of the input concentration of cytokinin, we have different stable levels of output. This can be seen in Figure 5, where the type A ARR and Wuschel levels show multistability, and in particular type A ARR levels are high within a specific concentration region of cytokinin, suggesting that as a single input determinant, cytokinin could perhaps function as a regulator of several biological processes due to the underlying network. Other questions we are pursuing through modeling are: What are the dynamical consequences of several different A, B type RR's, i.e. is it possible to obtain a multilevel switch perhaps with several thresholds of cytokinin (analogous to a staircase)? How does the system avoid crosstalk? A class of the cytokinin receptor is bifunctional. How does this system adapt to stochastic fluctuations?

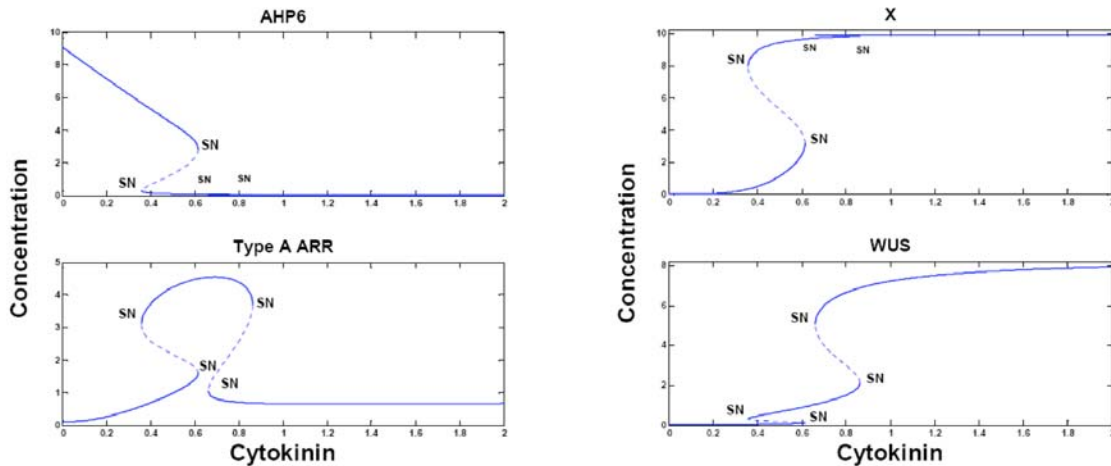


Figure 5: The steady state levels of AHP6, the X gene which suppresses AHP6, type A ARR and Wus, as a function of cytokinin levels. SN denotes saddle-node bifurcation. There are two sequential switching events which occur as cytokinin levels are increased. In particular type A ARR levels are high between a range of cytokinin suggesting that only within this range of cytokinin, specific processes which require type A ARR, could occur.

2.3 Regeneration (Gordon and Chickarmane):

What determines the patterns of root/shoot formation when callus is induced by hormone media to form new shoot apical meristems, and thereby regenerate plants? When root tips are grown in shoot inducing media, after a period of two weeks, shoots are formed at specific locations (Gordon et al., *Development* **134**, 3539-3548, 2007). We are interested in finding out if there is a self-organized process which determines these locations. Experiments, in which the expression of two important transcription factors, CUC2 and WUSCHEL are monitored, prior to the formation of shoots, appear to be correlated to the shoot formation regions (Gordon et al., 2007). It is also known that relative levels of auxin and cytokinin determine the formation of roots and shoots. We postulate that the relative hormone levels which act upon and get further regulated by an underlying genetic network, which in this case involves CUC2 and WUSCHEL, can lead to pattern formation of roots/shoots. Thinking along these lines, we have constructed a model of a regulatory network, which is shown below, in Figure 6.

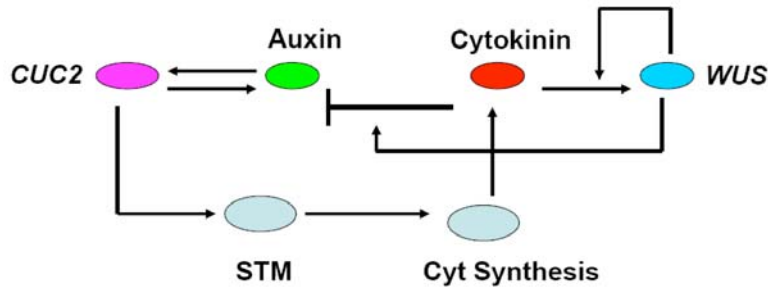


Figure 6: The regulatory network showing auxin and cytokinin acting upon the CUC2 and WUS genes. Auxin activates itself through its action on CUC2, but also induces cytokinin through STM (which synthesizes cytokinin). Cytokinin in turn is thought to negatively regulate auxin in addition to having positive feedback interactions with WUS (the previous section). The net result is a classic activator-inhibitor model.

The network shows CUC2 and WUSCHEL, and their interactions with the hormones auxin and cytokinin, respectively, which are both of a positive nature. The core circuit suggests that auxin and cytokinin function as an activator-inhibitor pair, which can lead to robust pattern formation. Patterns are obtained however, only if we assume that auxin diffuses at a rate much slower than cytokinin. This assumption is consistent with our understanding of auxin transport, which we know acts against auxin gradients by transport proteins, namely PIN1, which effectively reduces auxin diffusion. In Figure 7, we show a typical simulation which shows peaks of auxin surrounded by broader peaks of cytokinin,

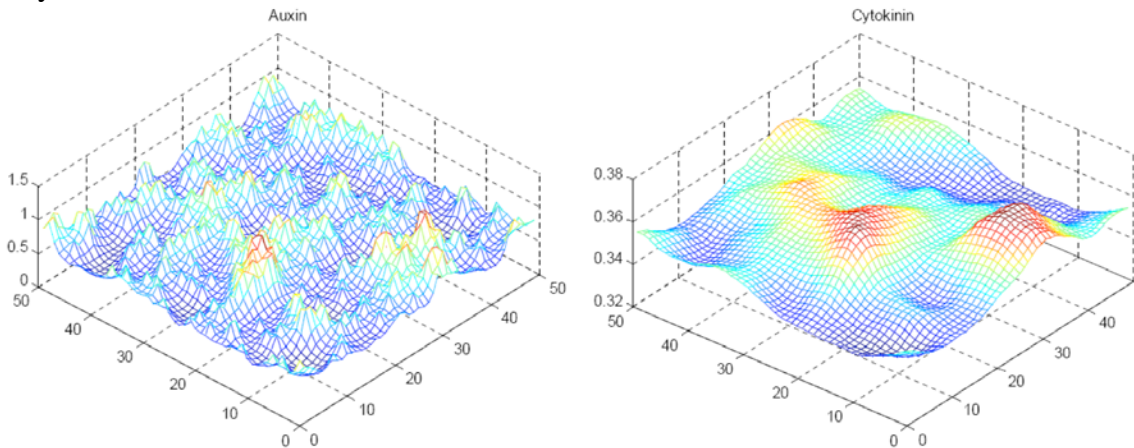


Figure 7. The regulator network shown in Figure 6 is converted to a set of reaction-diffusion equations, which are then solved for the steady state values of auxin and cytokinin. The plots show auxin and cytokinin concentrations as a function of space (in 2D).

for a 2D version of the reaction-diffusion system. Currently we are exploring the typical length scale of the pattern, as a function of the various feedback links, to study how the different interactions determine the size of the patterns. This we believe will be able to inform us about which regulatory links should be tested. For the future, we plan to further develop the model by including active transport of auxin due to PIN1, which should have the consequence of changing the effective diffusion, as discussed earlier, and hence can be further tested as a means to regulate the spatial extent of shoot formation. Through

experiments, we are currently testing several links of the regulatory network discussed above.

2.4 Homeostasis of stem cell numbers (Chickarmane)

The shoot apical meristem, which is located at the tip of the shoot, houses stem cells. It is a veritable fountain of youth, since it provides differentiated cells to form lateral organs, as and when they are required by the plant. It is a fascinating question, as to how the number of stem cells is maintained, by signaling and regulatory interactions between these cells and other more differentiated cell populations. Genetic studies in our laboratory have revealed one piece of this puzzle, which sheds light on a negative feedback mechanism, whereby cells located below the stem cells (organizing center--OC), maintain stem cells (forward loop), and where the stem cells somehow down-regulate the activity of the OC cells (backward loop). Specifically, cells re-specify from neighboring cell populations back into stem cells, when the backward loop of the feedback mechanism is interrupted.

To uncover other possibilities of regulation and general principles of homeostasis, we are employing a computational approach. We have developed population-based models that keep track of the number of cells of each population, where the rate of transitions from one population to the other is defined by the nature of the regulation. Through these population models we seek to identify which types of regulatory interactions can give rise to homeostasis. This would provide hypothesis, which we will use to test against the results of genetic experiments. In Figure 8, we show two such models which suggest either that cell specification can be controlled (model 1) or cell proliferation can be controlled (model 2).

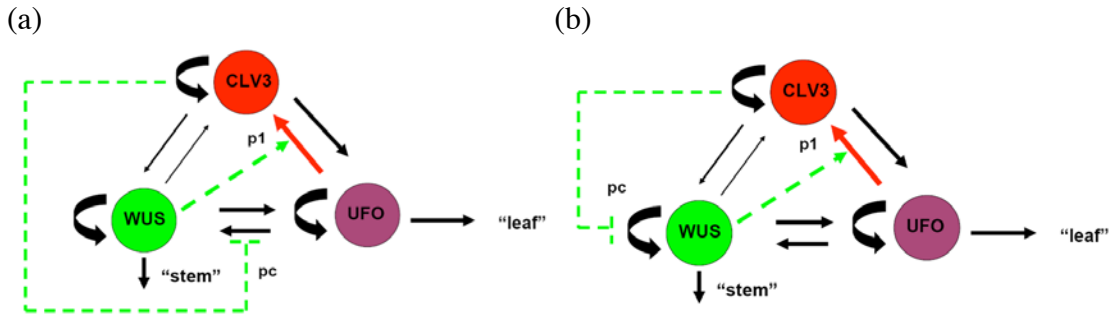


Figure 8. Two models which show regulatory schemes, for cell numbers, by which the CLV3, UFO and WUS expressing cells convert from one cell type to the other, with some of the rates depending on their cell numbers. Some of the links are common to both models, in particular those that make WUS and UFO cells ultimately go into forming the stem and leaves, respectively. Experiments in our lab suggest that CLV3-expressing cells get respecified from the UFO-expressing cells, and this rate is controlled by WUS-expressing cells. The two main hypotheses are, (a) Respecification: The CLV3 cells are hypothesized to control the rate of transition of the UFO cells to WUS-expressing cells. (b) Proliferation: The proliferation rate of WUS-expressing cells is controlled by the CLV3 cells.

The population models are described by differential equations, which can be used to compute the steady state cell numbers as a function of various parameters of the model. Two such parameters are essentially: how do cell numbers vary with respect to loss/gain of function of CLV3, and to loss/gain of function of WUSCHEL? In Figure 9, we plot

the cell numbers as a function of these parameters, which suggest that either extinction, or explosion of the cell numbers in the meristem, which agrees well with experiments.

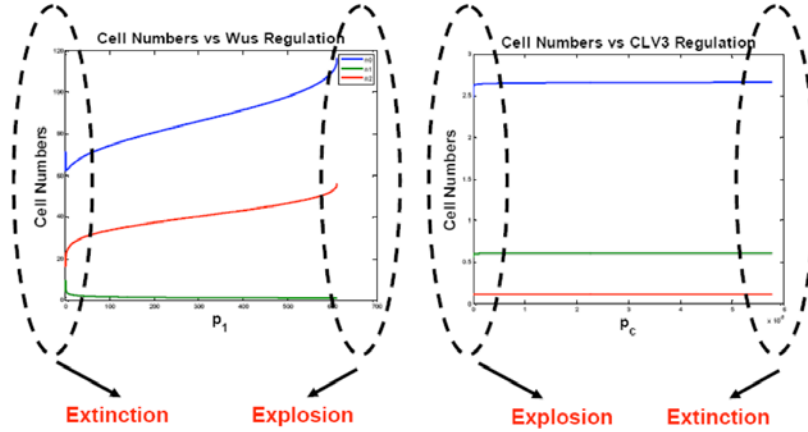


Figure 9: Based upon the schematics in Figure 8, we have described the evolution of the CLV3, UFO and WUS (n_0 , n_1 & n_2) cell numbers by coupled nonlinear differential equations. The equations contain parameters two of which correspond to loss/gain of function of CLV3 (parameter p_c), and loss/gain of function of WUS (parameter p_1). The plots show the steady state values of the cell numbers as a function of these parameters. In particular gain of function of WUS leads to a larger meristem (explosion) whereas loss of function of WUS leads to a small meristem (extinction). Similarly loss/gain of function of CLV3 leads to larger/smaller meristem, results which seem to be consistent with experiments.

The population models are amenable to a stochastic treatment, which would answer the question, as to the mean exit time for extinction of the meristem, i.e when the cell numbers go to zero. In Figure 10, we show a stochastic simulation of cell numbers which we then use to compute quantities such as the mean exit time, and the power spectrum of fluctuations. From an evolutionary standpoint, we would expect that a model of the shoot apical meristem would be robust against severe fluctuations in cell numbers, and hence these measures will allow us to differentiate between the two models.

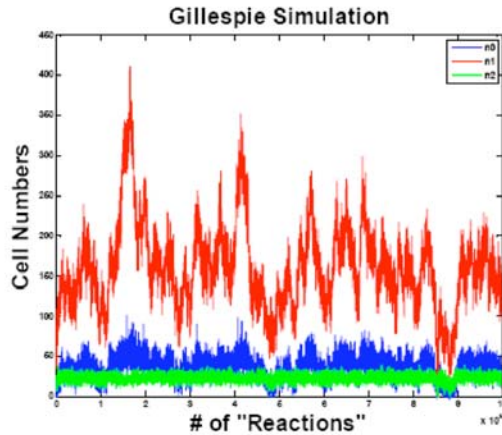


Figure 10. The figure shows a Monte-Carlo simulation (using the Gillespie algorithm) in which fluctuations of cell numbers can be clearly seen. Using these simulations we estimate the mean time for extinction/explosion, which could be used to differentiate the two models.

The next goal of this project is to scale this to a full spatial model, based upon a lattice, where each cell can be tracked independently. Such a combined computational/experimental approach we believe will significantly improve our understanding of the general paradigm of stem cells and their interactions with the niche.

2.5 Modeling of Cell Division (Shapiro, Heisler)

We have studied a model of cell division that takes into account several observations, notably the following four conjectures: (1) New cell walls are usually formed in a plane perpendicular to the principal axis of cell growth (Hofmeister's Rule, *J. Wissenschaft Bot.* 3:259-293, 1863); (2) New cell walls tend to form in a plane perpendicular to existing cell walls (Sach's rule, *Arbeiten des. Botanisches Institut Wurzburg*, 2:46-104, 1878); (3) The plane of division tends to correspond to the shortest path that will halve the volume of the mother cell (Errera's Rule, *Botanisches Centralblatt*, 34:395-399, 1888); (4) the planes of cell division tend to be staggered and avoid 4-way junctions (Sinnot & Bloch, *Am. J. Bot.*, 28:607-617, 1941). More recently it has been observed that prior to cell division microtubules and actin filaments form spindles that connect the nucleus with the nearest point on each neighboring cell wall. Because these spindles are under tension they tend to move away from vertices; one pair of these spindles coalesces into the pre-prophase band that marks the eventual site of cell division. (Picket-Heaps, *J. Ulstruct. Res.* 27:24-44, 1969; Flanders et al, *J. Cell Bio.* 110, 1111-1122, 1990; Goodbody, Ververloo and Lloyd, *Development* 113, 931-939, 1991). In our two-dimensional model we first identify all possible spindles by constructing line segments from the center of mass to the nearest point on each cell wall. In most cases these spindles will intersect the cell wall at a 90-degree angle, but in some cases they will intersect at a vertex. If the location of this vertex is not a local minimum distance (e.g., a small perturbation in *each* direction away from the vertex should lead to an increase in distance from the centroid), that particular spindle is removed from the list of candidate spokes. Then all possible combinations of spokes that meet at obtuse angles (angles greater than 90 degrees as measured at the centroid) are considered as possible division spoke-pairs. This set of spoke pairs is narrowed down by minimizing a potential function that depends on three factors, and which is calculated as the sum of each of the three different potentials: (1) an "area potential" that is zero when the two daughter cells have equal area ($VA=(A1-A2)/(A1+A2)$, in absolute value); (2) a "length potential" that is minimized when the sum of the lengths of the two spokes is minimal ($VL = (S1+S2-2b)/(2a)$, where S1 and S2 are the lengths of the spokes, and a and b are the major and minor radii of an ellipse of equal area to the cell that best fits the vertices); and (3) a "perpendicularity potential" that measures the relative perpendicularity of the two spokes to the direction of cell growth ($VP = \text{sum of the absolute values of the dot products of the spokes with the growth direction vector}$). The direction of cell growth is determined by calculating the singular value decomposition of a least-squares fit of the transformation matrix that takes the set of all vertices at one time point to a second time point just before cell division (Goodall and Green, *Bot. Gaz.* 147(1):1-15, 1986). These three factors can be added with different weights and used to predict the location of the cell division plane by minimizing the total potential over all allowed spoke pairs ($a*VA + b*VL + c*VP$ for some set of three numbers a, b, and c). This is illustrated in

Figure 11, which evenly weighted all three factors (a, b, and c all equal to one). The data was taken from (Heisler et. al. Curr. Biol. 15:1899-1911, 2005).

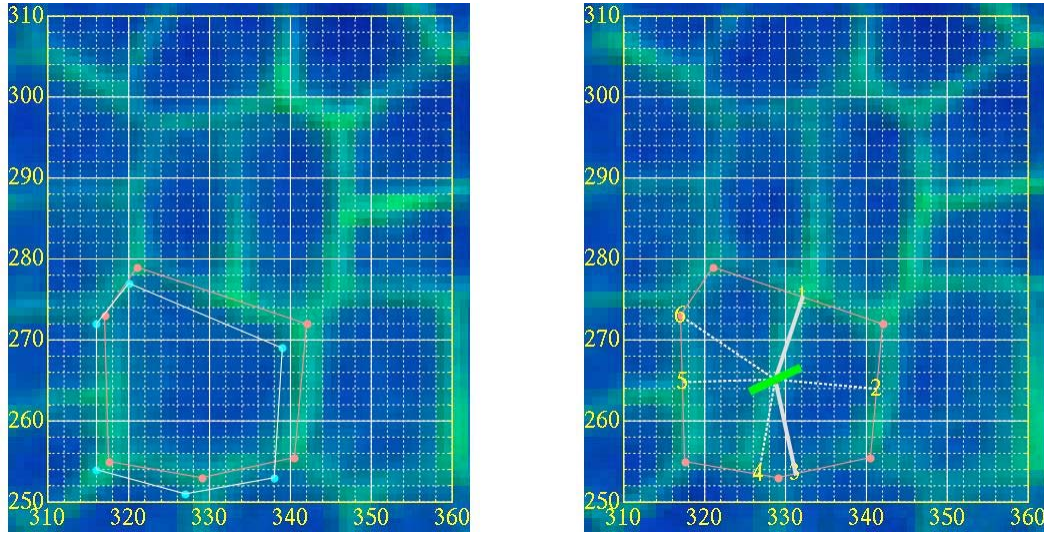


Figure 11. Left: observation of cell vertices at two time points just prior to cell division. Right: candidate spokes (dashed line); direction of cell growth (green bar); predicted pair of spokes that determine cell division (spokes 1 and 3, white line); superimposed on the actual post-division cell, showing the correctly pictured line of cell division.

3. Image Analysis

3.1 Sepal Live imaging (Roeder)

Last year we developed the technique for live imaging the nuclei of lateral organs, in this case sepals. This year we have improved the technique by adding visualization of the plasma membranes and taking images at shorter time intervals (6 hours instead of 12).

In our earliest live imaging sequences we have observed that approximately 8 files of cells in the floral meristem give rise to the sepal. In this initial phase during the formation of the sepal primordia, all of the nuclei are approximately the same size, indicating that all cells are still 2C or 4C depending on their stage in the cell cycle (Figure 12, 0 hours). From the results of the computational model, I first predict that giant cells should stop dividing and start endoreduplicating early in sepal development. I observe that from this early time point the giant cells never divide and their nuclear size increases indicating that they are endoreduplicating (Figure 12, note arrows and **nuclear size**). The second prediction is that the smaller cells should continue to divide while the giant cells endoreduplicate. During this same three-day period, we observe that the smaller cells undergo 1 to 4 rounds of division (Figure 12). Contrary to the model, we observe that the cell cycle periods of mitotic cells are not uniform. In the coming year we will revise our model to take into account varying cell cycle times. The final prediction is that the area of one giant cell should equal the area of a whole neighboring lineage if the growth rate of small cells and large cells are equal. We observe that giant cells are approximately equal in size to the entire neighboring small cell lineage (Figure 12, 72 hours).

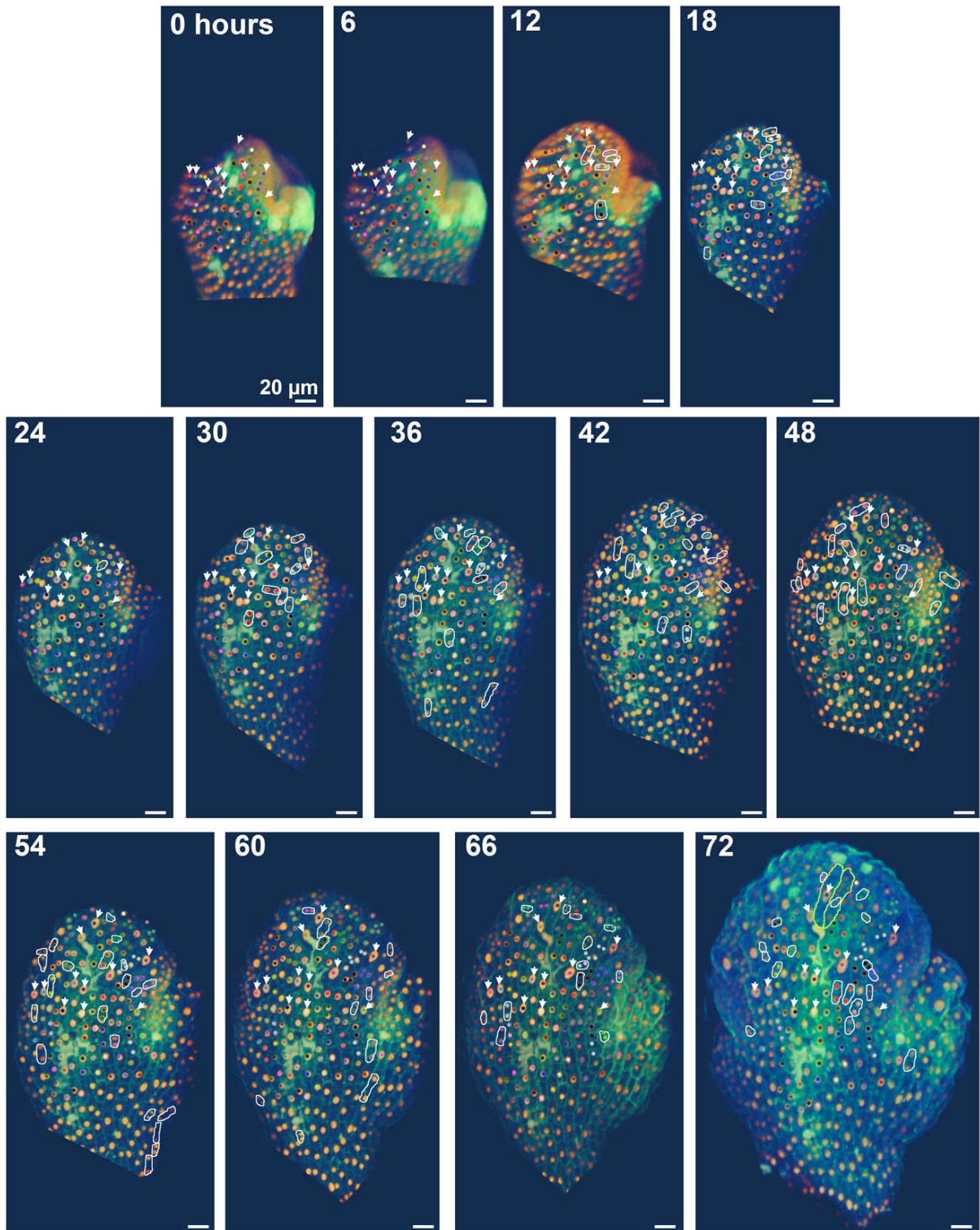


Figure 12: Live imaging of wild type sepal development

A single flower was imaged every 6 hours. The nuclei in the epidermal cell layer were visualized with a fluorescently tagged histone (*ML1::H2B-mYFP*) shown in gold. The

cell walls were stained with Propidium iodide shown in green (dead cells are also labeled). The 3D confocal stacks generated at each time point were processed with the Amira software package and the images shown are the final cropped, registered, volume rendered output. To analyze the pattern of cell division and endoreduplication, the lineage of each of the cells was tracked. At time 0 each cell was marked with an individual colored dot. At subsequent time points that cell and all of its progeny receive a dot of the same color. Cell divisions are marked in the time point following the division by a white circle connecting the two daughter nuclei. Note that the giant cells (indicated with arrows) never divide throughout the 72-hour period. At time 0 the giant cell nuclei are the same size as surrounding cells suggesting that they have a similar DNA content and have not yet started to endoreduplicate; however, by the end of the image sequence the giant cell nuclei are enlarged relative to their neighbors suggesting that they have undergone endocycles. Also note that the growth rate of giant cells and neighboring small cells appears to be equivalent.

3.2 Processing of live imaging data (Burl)

Over the past year, image analysis techniques have been developed and applied to new datasets help answer key biological questions relating to sepal development in *Arabidopsis*.

An automatic nucleus segmentation algorithm was developed to provide improved accuracy in identifying nuclei in fluorescent CLSM images and stack projections. The technique uses local filtering, thresholding, and connected components to initially identify blobs. Features extracted from the blobs, such as the number of local maxima and deviation of the boundary contours from an ellipse, are used to determine whether a given blob should be split into smaller blobs. Figure 13 shows nuclei detected by the algorithm (in randomly selected colors) superimposed on an image of the corresponding cell membranes.

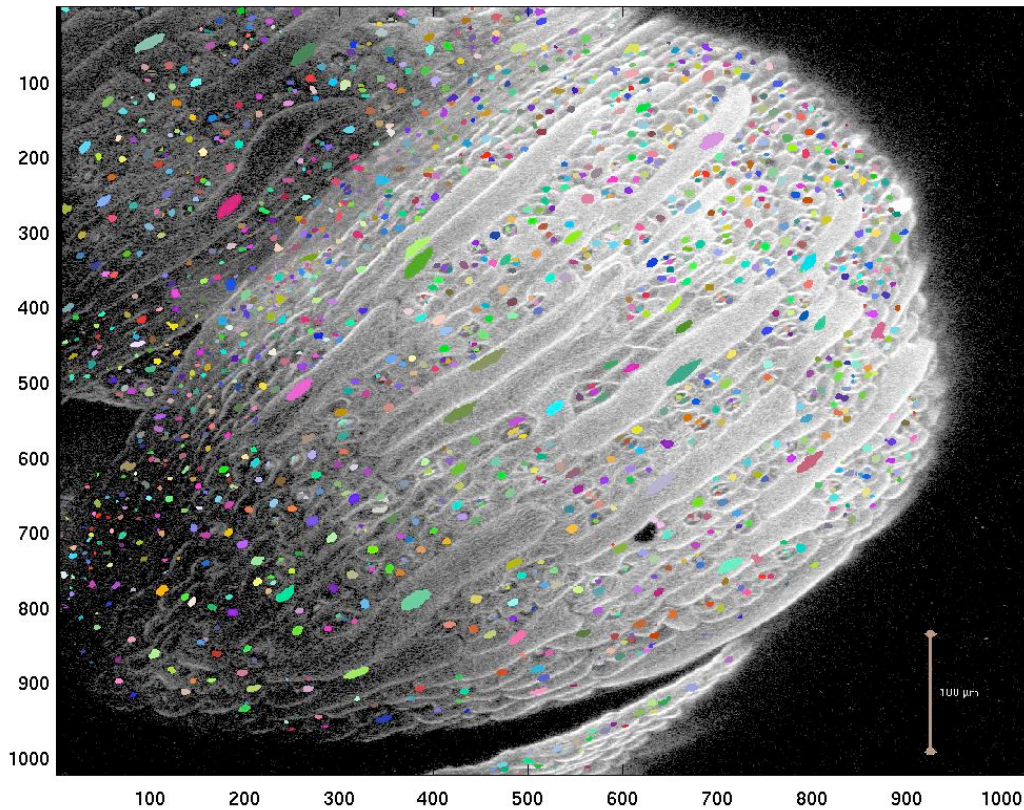


Figure 13. Nuclei detected by the nucleus segmentation algorithm (in randomly selected colors) superimposed on an image of the corresponding cell membranes.

Since the formation of giant cells is one of the most striking features in the developing *Arabidopsis* sepal, a variety of tools for statistical analysis of the segmentation images was developed. For example, one tool determines ellipse moments and uses these moments to determine a pseudo-volume, V , for each nucleus. Looking at histograms of $\log_2(V)$ for different *Arabidopsis* mutants, which externally show differences in their giant cell structures, can be used to quantify specific properties. Figure 14 shows normalized histograms of nucleus pseudo-volume for wild type, as well as the siamese-related 1 (*smr1*) mutant and the E10-19 mutant.

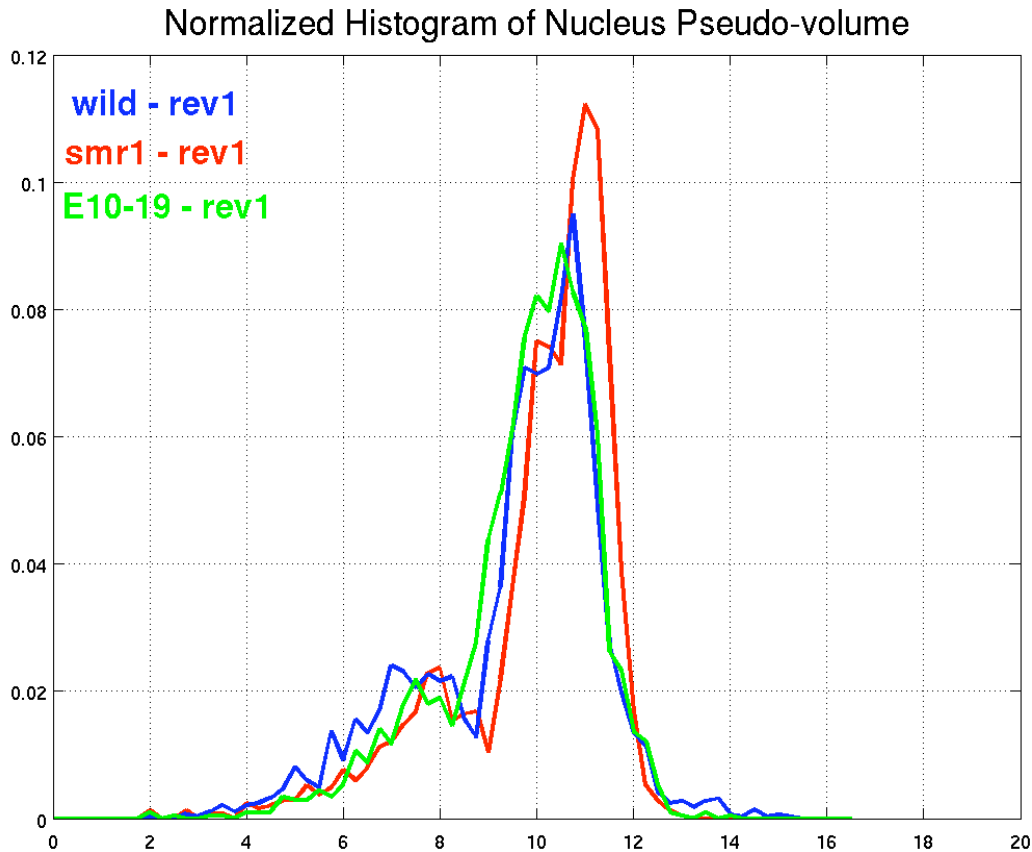


Figure 14. Normalized histograms of nucleus pseudo-volume for wild type, as well as the siamese-related 1 (smr1) mutant and the E10-19 mutant.

The spatial distribution of giant cells and non-giant cells is also of interest. A graph showing which cells have a shared wall with which other cells captures the spatial topology. Floyd's algorithm was implemented to compute the "hop distance" between all pairs of cells. Because of the elongated shape of the giant cells, the hop distance is likely to be more relevant for study of spatial relationships than simple Euclidean distance. Figure 15 shows the color-coded hop distance between the central red cell and the other cells (e.g., the dark purple cells are two hops from the central red cell).

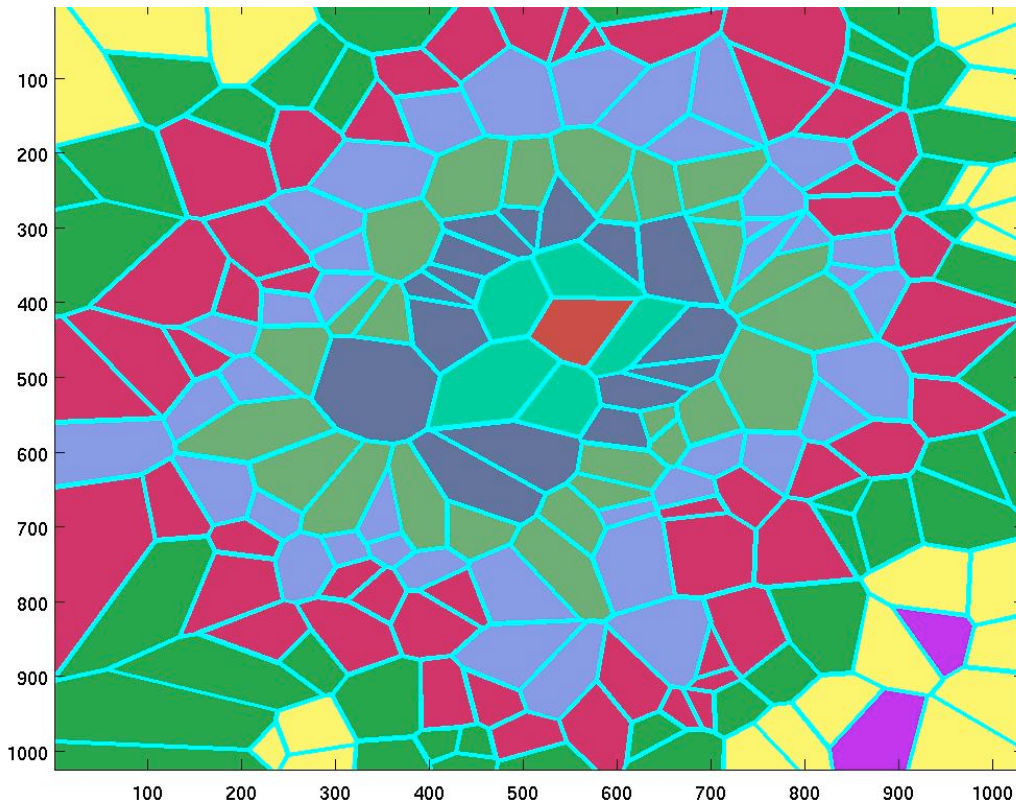
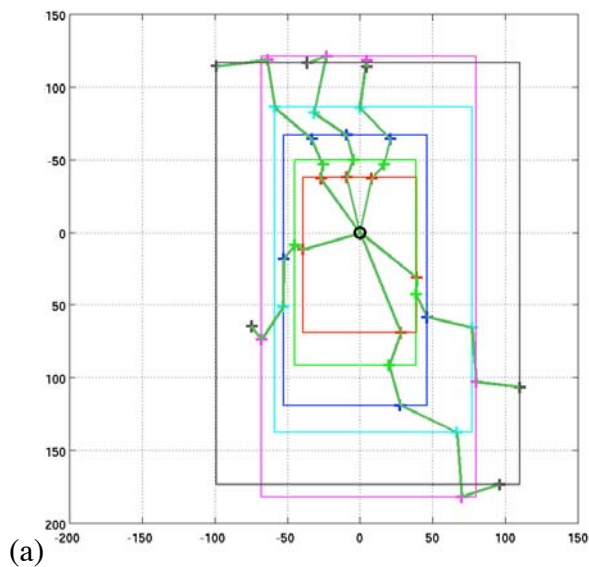


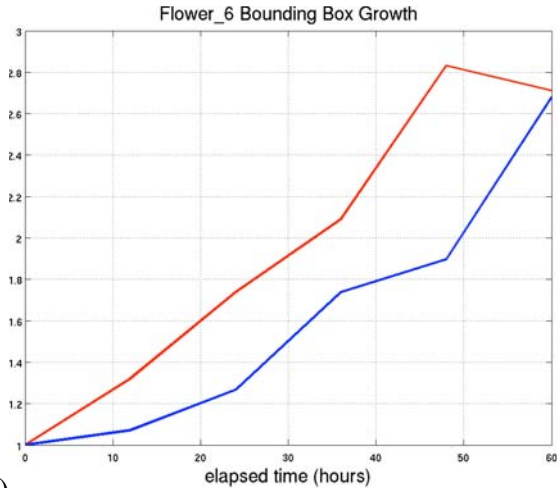
Figure 15. Color-coded hop distance between the central red cell and the other cells (e.g., the dark purple cells are two hops from the central red cell).

In addition to analysis of static sepal images, a major thrust over the past year has been the study of time sequences. The ability with live imaging to observe the same developing specimen at different time points is a huge advance over previous imaging techniques. Algorithms were developed that can take nucleus tracking results and assign lineage labels to the nuclei. Figure 16a shows the initial nucleus labels assigned to nuclei in a sepal that is at an early stage of development. Figure 16b shows the lineage labels approximately 8 days later. Figure 16c shows the destination of various nuclei from the early sepal, with the triangle markers representing the position of the nucleus (or its descendant) after 8 days of development. The vectors are color-coded to represent the number of descendants produced by the original nucleus, e.g., red represents a nucleus that persisted without dividing, and green represents a nucleus that divided once to form two daughter cells.

original nucleus, e.g., red represents a nucleus that persisted without dividing, and green represents a nucleus that divided once to form two daughter cells.

Tools for more detailed growth studies and estimation of growth rates were also developed. One tool uses singular value decomposition (SVD) of the estimated affine transformation between successive frames in a time sequence to establish principal growth axes and rates of growth along these axes. The growth curves are well-modeled by exponential functions (equivalent to a compound interest model). Figure 17a shows an alternate analysis based on aligning sepal images according to a macroscopic coordinate system for the entire sepal and looking at the growth of an axis-aligned bounding box. All markers of a given color represent the positions of a handful of nuclei at a specific time point. Each radial olive green line connects all instances of the same nucleus over time. The colored rectangles show the growth of the bounding box over time. Figure 17b shows the corresponding cumulative growth curves with red representing growth along the long axis of the sepal and blue representing growth perpendicular to the long axis. (Note that the curves are normalized to start at 1 when $t=0$; we are mainly interested in the growth factor obtained from an exponential fit to the curves rather than the absolute sizes versus time.)





(b)

Figure 17. (a) This figure shows an alternate growth analysis based on aligning sepal images according to a macroscopic coordinate system for the entire sepal and looking at the growth of an axis-aligned bounding box. All markers of a given color represent the positions of a handful of nuclei at a specific time point. Each radial olive green line connects all instances of the same nucleus over time. The colored rectangles show the growth of the bounding box over time. (b) This graph shows the corresponding cumulative growth curves with red representing growth along the long axis of the sepal and blue representing growth perpendicular to the long axis. (Note that the curves are normalized to start at 1 when $t=0$; we are mainly interested in the growth factor obtained from an exponential fit to the curves rather than the absolute sizes versus time.)

To verify that the giant cells are endoreduplicating, we measured the nuclear area over time. In plants the nuclear area is proportional to the DNA content. We observe, that while all the nuclei are of a similar size at time point 0 indicating that they are all 2C, the giant cell nuclei (colored) increase in size over the period of the time-lapse image. In contrast, the dividing nuclei (black) remain within the same size range throughout the time interval indicating that they have not endoreduplicated. Note that in the last time point at 72 hours, the sepal rotates, which causes the absence of nucleus 6 (magenta) from view and the apparent shrinkage of nucleus 3 (blue).

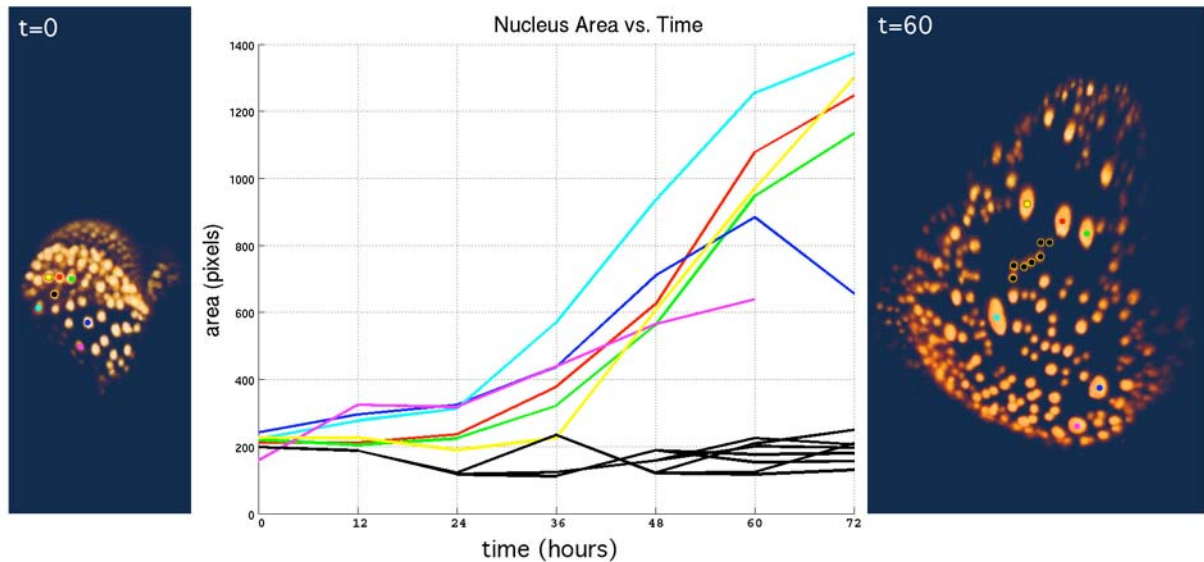


Figure 18. Giant cell nuclear size increase versus time. The colored curves show the growth of giant cell nuclei over time. The black curves represent a control test which shows that the (regular) dividing nuclei remain within the same size range throughout the time interval indicating that they have not endoreduplicated.

3.3 Filtering: improving quality of microscopy images (Cunha)

Images generated in optical and electron scattering microscopy inevitably contain noise, which might prevent a straightforward computational image analysis. The *in vivo* confocal images acquired during the development of the *Arabidopsis thaliana* are not an exception. Noise is present throughout the entire image stack. We have greatly benefited from removing noise prior to further image processing. Robust image denoising has significantly helped us in the development of a semi-automatic method for segmenting cell membrane and cytoplasm. Denoising has also allowed us to clearly visualize and identify the geometries present in an image, as for example the shape of cell walls before and after mitosis, which is a valuable measure in the investigation of cell growth.

We have developed a robust and efficient algorithm for nonlocal image denoising [1,2], which is a rewriting of the recently proposed nonlocal means filter of Buades, Coll, and Morel [2]. Our approach and efficient implementation on contemporary shared memory multicore computers enabled us to produce results much faster than competing schemes with either superior or equally good results. The method works by computing for each pixel in the image a weighted average intensity and it takes into account the distance between patches around the pixel being modified and its neighboring pixels in both Euclidean and intensity spaces. The underlying principle justifying the remarkable success of the method is that an image itself contains enough redundant information to boost its signal.

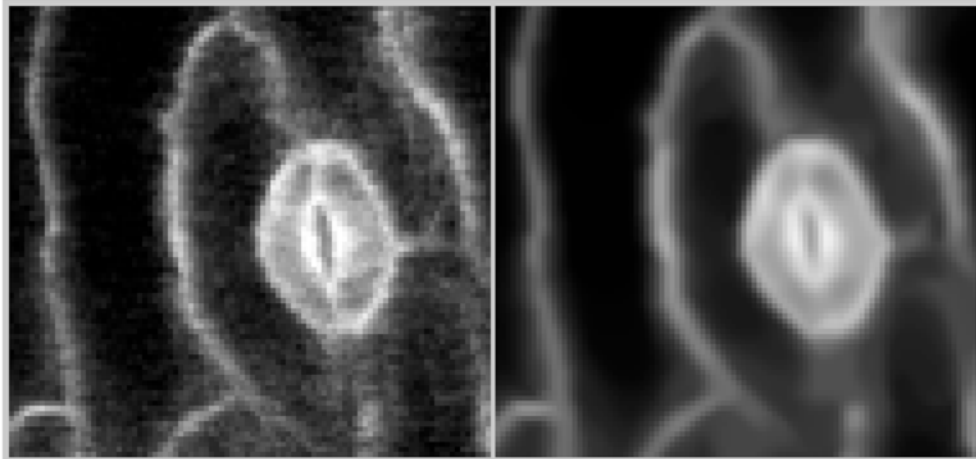


Figure 19: This figure shows the noisy and denoised versions of a tiny piece of a much larger image of guard cells in a sepal, magnified 8x from the original image. Note the sharpness of cell walls after denoising and the almost homogeneous intensity in the cytoplasm. These are typical characteristics of results obtained with our filter, which contribute to a great extent in segmentation.

Timings for filtering images of different sizes					
image size	256 ²	512 ²	1024 ²	2048 ²	4096 ²
time (s)	0.07	0.35	1.54	6.05	26.32
scalability	–	5.0	4.4	3.9	4.4

Table 1. Timing for filtering images of different sizes. Filtering time scales linearly with image size, which is a desired property specially when working with large sized images typically produced by current microscopes. Note from the table above that small images are filtered in real time. This is convenient when we are only interested in a small portion of the overall image.

3.4. Segmentation: a fully automatic approach (Cunha)

We developed automatic and semi-automatic segmentation methods to determine sizes of sepals and cells.

In our completely automatic approach we adopted the Active Contours Without Edges model presented in [2]. The method works by splitting the image into regions each with a unique average intensity. Although there may be multiple disconnected regions there are only two distinct segmented areas, one representing the foreground and the other the background. The *interior* region corresponds to the region of interest, the foreground, while the *exterior* region represents the background. In theory, a pixel moves to a foreground region if its color is closer to the foreground color than the background color, and vice versa. The method is suitable for segmenting sepals because their natural color

is uniform or close to uniform when compared to the background intensity or we can stain them such that their color becomes almost homogeneous during image acquisition.

We have implemented the active contours segmentation program with robustness in mind and efficiency at this point is of secondary concern. We solve the Euler-Lagrange partial differential equation corresponding to the energy model using steepest descent. Although this can be excruciatingly slow for some problems, it gave us much control on the propagation of the level set curve that defines the interface between interior and exterior regions. Since we are mainly concerned with computing areas of blob type objects, like sepals, we can reduce images to an affordable size prior to segmentation without compromising results. Once we get a mask in a reduced image we scale back to original size to obtain true measurements. In practice, we experimented a CPU wall clock per iteration very affordable (less than 1 minute per sepal) and we could segment 16 sepals at a time using our multicore platform.

The winning sepal segmentation approach consisted of combining a strong staining with mixing of mathematical morphology clean up procedures and active contours segmentation method. In a few cases sepals did not have a uniform color thus presenting difficulties to have a single segmented region (see Figure 21). By *strongly coloring* sepals and removing spurious data from the images using mathematical morphology operators (see Figure 22) we were able to generate accurate masks for sepals, from which we could automatically compute area sizes. This procedure entirely eliminated manual interventions to correct results. Validation of automatic results showed errors below 3% (given that the manual segmentation is accurate, an assumption we can certainly dispute).

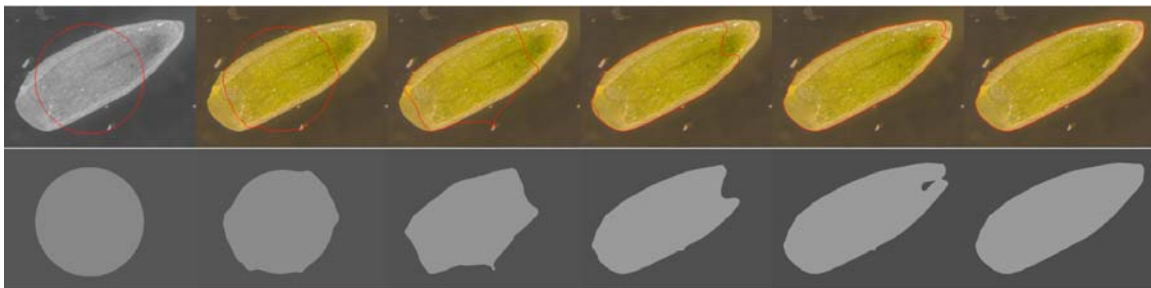


Figure 20. We have segmented sepals using the active contours without edges model [3]. The top row shows a few steps of the propagation of the level set curve (in red) enclosing the region of interest, from start (circle) to final configuration. The bottom row shows the respective evolution of the segmented region. The sepal area is computed from the final binary mask (bottom right image).

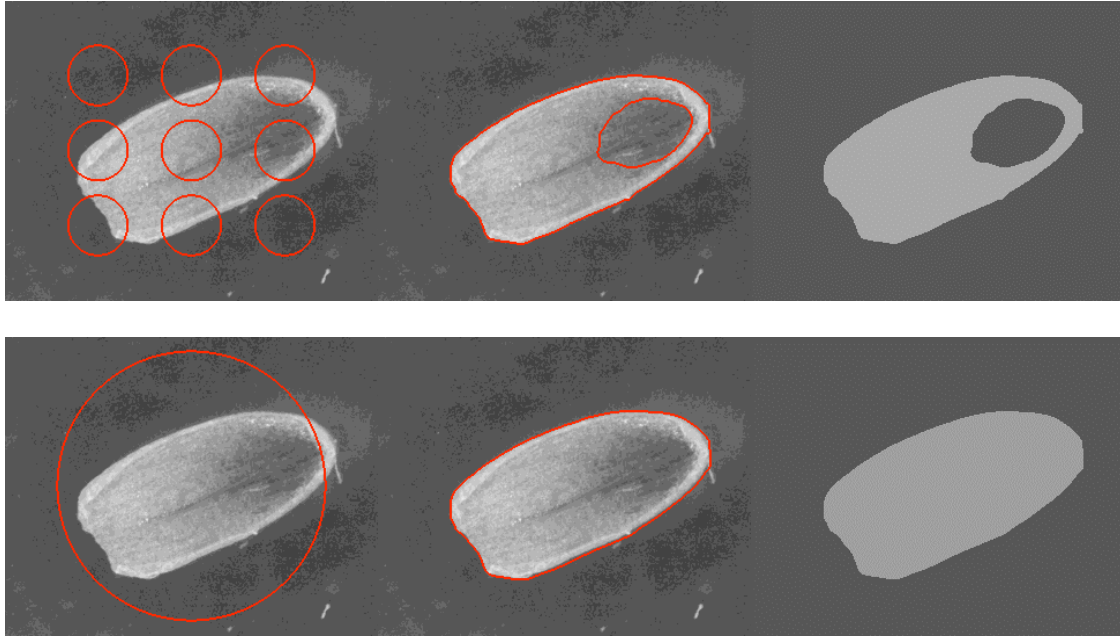


Figure 21. Segmenting sepals with a soft rubber might create more regions than necessary. (Top row) A small area within the sepal has approximately the same average intensity as the region exterior to the sepal leading the soft rubber to split into two pieces and create an undesired hole as seen in the top right picture. (Bottom row) We solve this problem by strengthening the rubber and starting from a level set curve covering approximately the whole sepal. The rubber shrinks and converges to the right response without breaking into pieces. The rubber stiffness and its initial contour are thus important parameters of the problem.



Figure 22. A combination of right imaging and segmentation tool led us to a fully automatic segmentation method for sepals, even when small aberrations are present in the images. Sepals were stained such that their color is almost completely homogenous throughout thus eliminating the problem of multiple regions with same average intensity shown in Figure 21. We use mathematical morphology operators to remove the spurious thin features present in these new images (left picture) and prior to run our active contours segmentation program. The final mask is accurate and just a few iterations are needed to converge to a stable solution.

3.5. Segmentation: an assisted approach (Cunha)

The automatic segmentation of many neighboring cells, shown for example in Figure 23B, presented some difficult challenges. The usage of our active contours segmentation revealed leakages through cell walls in many places, hard to control in a satisfactory fashion. Spurious information coming from neighboring slices, non-uniform coloring, and most importantly the occurrence of cell walls with weak signals were the major impeding factors that prevented us from adopting our previously described automatic segmentation approach. These difficulties led us to develop an assisted segmentation method that in practice behaved much better than the automatic one for these types of images, and it required little user intervention to control the quality of results.

Note that although we developed what we think is a simple but robust method our success naturally depends on the quality of the acquired images. Highly deteriorated images would require a more sophisticated segmentation approach. But given that newer technologies can produce images with superior quality, our current methods are certainly applicable to them and higher rates of success are expected.

We adopted our assisted approach for segmenting images of the types illustrated in Figures 23 and 24. We stress here that filtering has played a major role in facilitating the development of this approach. Filtering significantly enhanced edges in the images while smoothing flat areas and judiciously throwing away as much noise as possible.

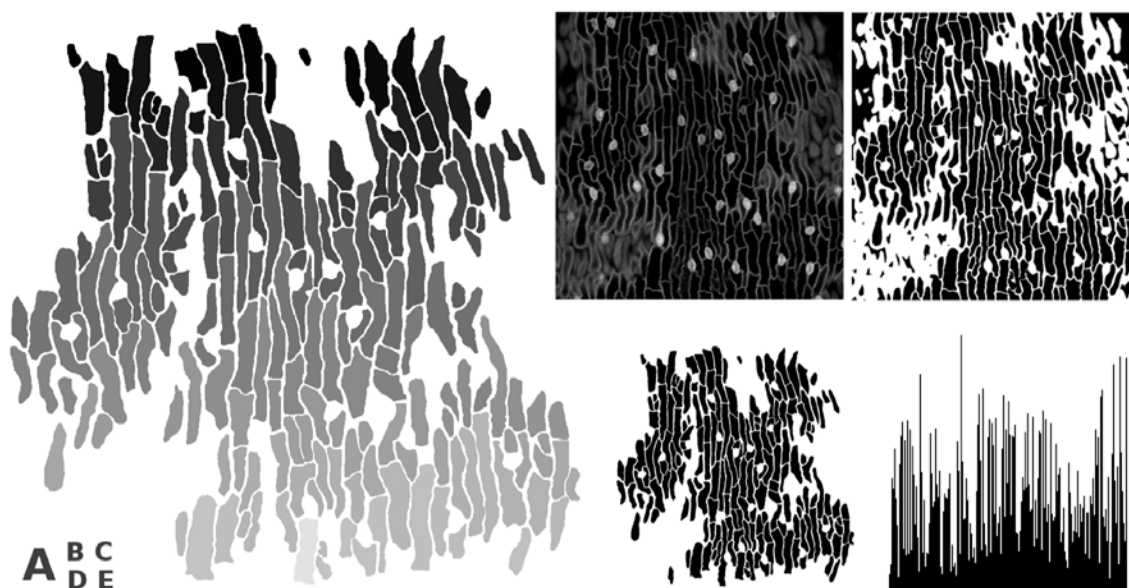


Figure 23. We developed an assisted segmentation procedure to measure cell size where relatively little manual intervention is required to segment cells. The image in (A) shows a large number of the cells present in (B), each cell colored with a different gray color. In (B) we have the result after filtering an original slice from a confocal image (not shown)

using our fast nonlocal mean filter. Denoising leaves cells with uniform or close to uniform dark colors throughout, easily distinguishable from cell walls that are much lighter. A simple threshold applied to the filtered image approximates very well the cell interior regions, shown in (C). But due to spurious information inherited from the acquisition process, a manual intervention is needed to discard those badly segmented cells (user visually selects and eliminates undesired masks). A set of clean cells is then created resulting in the image (D). Running a connected components program in this binary image produces the colored image in (A) whose histogram (E) gives us the area of each cell.

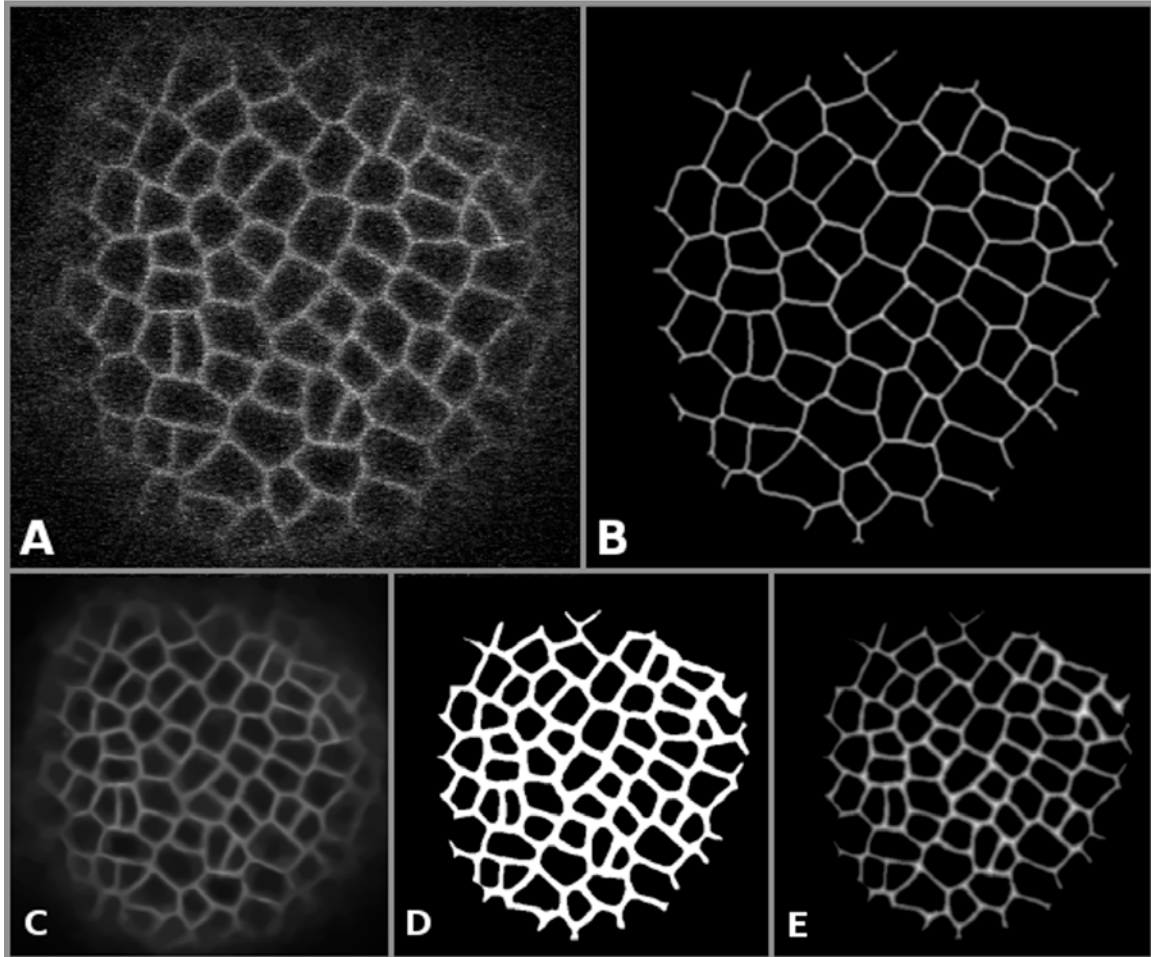


Figure 24. From images to geometric models of cell walls. We want to depart from the simplified, straight sided geometric model for cell walls to a more faithful model that closely mimics the observed data. This should ultimately impact the quality of plant growth simulation as we introduce finite element models that more accurately represent reality. The image in (A) is a slice from a confocal stack, very noisy, but with enough information for us to construct an equivalent image (B) showing clearly the cell walls in (A). We achieve (B) after the following image processing steps: we denoise (A) with our robust filter [1,2] and obtain (C) whose cell interiors and walls are very distinguishable and clean of noise. (D) is the gray color threshold of (C) giving the cell walls a thickness.

We compute the distance transform [5] of these walls and obtain (E). We extract the ridges of (E) which are unique one pixel wide lines. The ridges represent the central lines, the skeletons of cell walls and they have all the necessary information to construct decimated splines representing the wall edges. The image in (B) is a slightly blurred version of the ridges so to allow an easy visualization otherwise difficult with one pixel wide lines. We are currently working on methods to construct these decimated splines from the pixelated lines and build 3D cells from them.

References

- [1] J. Darbon, A. Cunha, T.F. Chan, S. Osher, G.J. Jensen, “Fast Nonlocal Filtering Applied to Electron Cryomicroscopy”, in IEEE International Symposium on Biomedical Imaging, pp. 1131-1134, Paris, France, May-14-17, 2008.
- [2] A. Cunha, J. Darbon, T.F. Chan, S. Osher, “Fast Nonlocal Means Filtering”, in SIAM Imaging Sciences Conference, July 7-9, 2008, San Diego, CA.
- [3] A. Buades, B. Coll, J.M. Morel, “A review of denoising algorithms, with a new one”, SIAM Journal on Multiscale Modeling and Simulation, 4(2) pp. 490-530, 2005.
- [4] T.F. Chan, L. Vese, “Active Contours Without Edges”, IEEE Transactions in Image Processing, 10:266-277, 2001.
- [5] R. Fabbri, L.F. Costa, J.C. Torelli, O.M. Bruno, “2D Euclidean Distance Transform Algorithms: A Comparative Survey”, ACM Computing Surveys, 40(1), pp 2:1-2:44, 2008.

4. Mathematical and Software Tools for modeling

4.1 Mathematical tools for modeling

In order to compare the Dynamical Grammars (DG) modeling framework developed within the Computable Plant project [Mjolsness and Yosiphon 2006] with others such as L-systems and P-systems, we examined the mapping of graph grammars into DG's and of geometric cell complexes into graph grammars. The first mapping requires a global object identifier (OID) parameter added to each simulated object, which can then appear as a mutable parameter in other objects thereby constructing a dynamic web or graph representation. But can graph grammars be mapped into the semantics of DG's, which is given in terms of time evolution operators, *without* the use of globally unique OID's? This question was pressed on us by Przemek Prusinkiewicz.

The answer seems to be a qualified yes. There is a direct mapping of the DG syntax for graph grammars to time-evolution operators, in which the symbolic OID parameters are reinterpreted as local and temporary object identifiers rather than global and permanent ones. And new syntactic constructs can be added to the language which omit such parameters entirely. All of this leads to a natural extension of DG's, which we call Dynamical Graph Grammars (DGG's), that may be convenient for developmental modeling. However, behind the scenes in the general expression for DGG time evolution operators that determines the validity of any simulation engine, a sum over global object indices is still required. It's not part of the language anymore, so of no concern to the users of the modeling language, but it remains part of the semantics of the language, and therefore important to inventors of simulation algorithms.

4.2 Software tools for modeling

Software Developed (Shapiro)

We have developed a the growzilla simulator, which implements the spring wall model in two dimensions. Cells are modeled as polygons, with springs connecting the two vertices at the end of each wall (see Figure 25). The resting length of the spring is increased in proportion to strain to simulate growth; the dynamics of a physics-based model of weak springs in a viscous medium is used to maintain cell shape as the wall lengths increase to match their resting lengths. Turgor pressure is simulated by a fixed outward force on each wall that is applied normally and split equally at each vertex. Tissues are implemented using a data structure that is composed of three parts: a list of vertex coordinates; a list of edges specified as vertex pairs; and a list of cells specified as lists of edges. Cell division is implemented with the model described elsewhere in this report, and occurs when the cell mass (area) passes a pre-specified threshold. Anisotropic growth and strain models are also implemented. In addition, the hypothesis that the cells stiffen in a direction perpendicular to cell growth, the direction of cell growth is used to dynamically determine the stiffness of the springs as a function of time. Figure 25 shows the end result of a simulation starting with a single hexagonal cell after twelve cell division using a

1:3:1 weight ratio (area:length:perpendicularity) of the model described elsewhere for cell division, incorporating the stiffness feedback model. Growzilla is built on a substrate of programs that includes the open source mathsml, xlr8r, and mergeinterpolation packages.

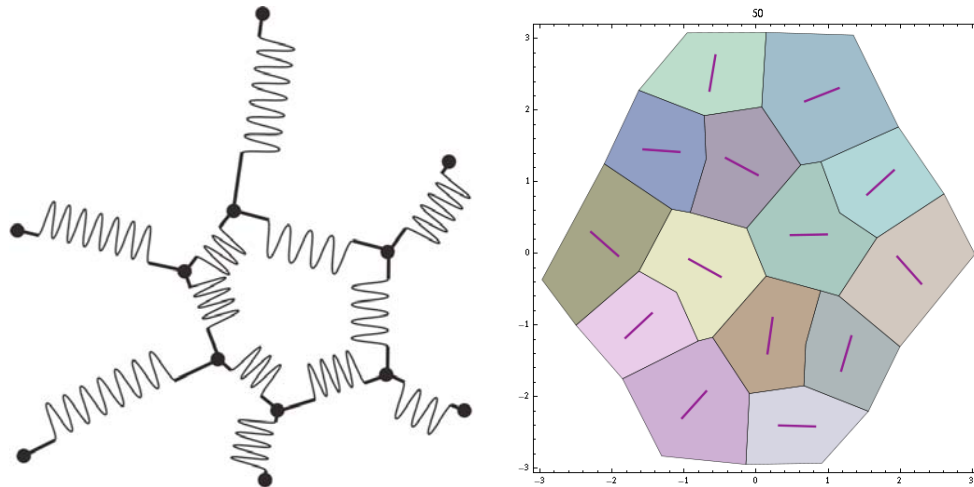


Figure 25. Spring wall model. Each cell is described by a network of springs around the edges. Right: result of applying the cell division model starting with a single hexagonal cell, after 12 cell divisions. The bars indicate growth direction.

Several other software packages were modified this year; (1) The xCellerator simulator, which is used to simulate biochemical networks via the automated conversion of reactions into differential equations and their numerical solution had several improvements: It was upgraded to compatibility with Mathematica version 6.0; install scripts for linux and Mac OSX were included in the distribution; a new option “BoundaryCondition” was added to allow simulations with time-dependent stimulations (instead of just at time equals zero); several improvements to improve efficiency were implemented. (2) The x20 simulator was developed to produce reactions in the organism file format and run simulations using the organism simulator. (3) The “MergeInterpolation” package was developed to aide plotting and merging of interpolation data overt different time spans that have different numbers of equations. MergeInterpolation is used by Growzilla. (4) Cellzilla/Mpower which is use to develop static simulations using a weak spring model and Voronoi geometry was upgraded to Mathematica version 6.

Reference

“Stochastic Process Semantics for Dynamical Grammars”, Eric Mjolsness and Guy Yosiphon. *Annals of Mathematics and Artificial Intelligence*, 47(3-4) August 2006.

5. Activities and Meetings

Computable Plant Annual Meeting, Caltech Kerckhoff Marine Lab (KML), Corona del Mar, California, Saturday, Nov 17, 8:30am - 4:00pm:

Schedule

Eric Mjolsness and Elliot Meyerowitz: Brief introductions
Adrienne Roeder (Caltech): Sepal biology and image analysis
Vijay Chikarmane (Caltech): Sepal model

10-11am:

Victoria Miranova (ICG): ODE root model
Guy Yosiphon (UCI): Dynamical Grammar root model
Break & discussion

11am-12 noon:

Sergey Nikolaev (ICG): Shoot Apical Meristem homeostasis and maintainance
Bruce Shapiro (ICG): Shoot Apical Meristem maintainance

Lunch

1-2pm:

Nadya Omelianchuk (ICG): AGNS database software
Tigran Bacarian (UCI): Image analysis software
Break & discussion

2-3pm:

Sean Gordon: Callus biology
Ilya Akberdin (ICG): Embryo model

3-4pm:

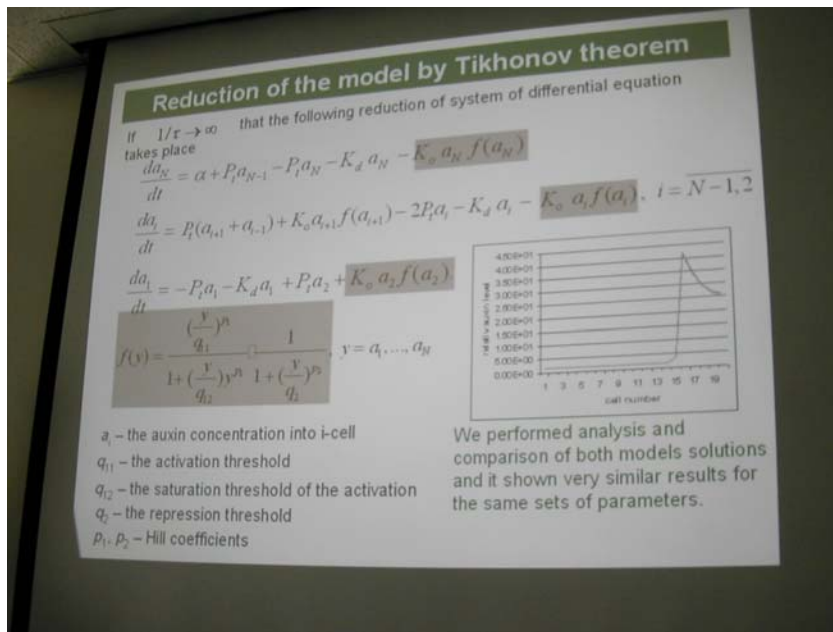
Discussion and opportunity for technical interchange.



Eric Mjolsness and Adrienne Roeder at KML.



Sergey Nikolaev, Victoria Mironova, and Ilya Akberdin (all from Institute for Cytology and Genetics (ICG), Novosibirsk, Russia) at KML. Also visiting from ICG were Vitali Likoshvai and Nadezhda Omelianchuk.



Some applied mathematics for root modeling at KML.

Spinoff meeting series: Computational Morphodynamics “supergroup meetings” at Caltech. First of the series:

Caltech Computational Morphodynamics Workshop
 21 May 2008, Powell-Booth 100, Caltech campus

09:00 AM	09:15 AM	Introductions
09:15 AM	09:40 AM	Meyerowitz Lab
09:40 AM	10:05 AM	Elowitz Lab
10:05 AM	10:30 AM	Asthaigiri Group
10:30 AM	10:45 AM	Break
10:45 AM	11:10 AM	Mjolsness Group
11:10 AM	11:35 AM	CACR
11:35 AM	12:00 PM	Discussion
12:00 PM	12:30 PM	Lunch
12:30 PM	12:55 PM	Boris Shraiman (UCSB)
12:55 PM	01:20 PM	Stathopolous Lab
01:20 PM	01:45 PM	Ingmar Riedel-Kruse
01:45 PM	02:00 PM	Coffee
02:00 PM	03:00 PM	Discussion



Caltech Computational Morphodynamics Workshop (May 21, 2008). Front row: unidentified, Anand Asthagiri, Elliot Meyerowitz, Vijay Chickarmane, Michael Elowitz, Boris Shraiman (KITP). Second row: Bruce Shapiro, Oren Schaedel, Marcus Heisler, Adrienne Roeder, Alex Cunha, Lauren LeBon, David Sprinzak, Chin-Lin Guo. Summarized at <http://computational-morphodynamics.net/meetings.html>.

6. K-12 Outreach

Grounding in Botany at the Huntington Botanical Gardens completed its fourth full year and we are in the middle of the fifth year's summer institute. The *Grounding in Botany* program continues to combine support with a grant from the Arthur Vining Davis Foundations. This summer and last we moved to a four-week format (four days a week). The program year began with a very successful summer course and was followed by five workshops scheduled through the 2007-2008 academic year. This summer's course will also be followed by five workshops through the 2008-2009 school year.

We continued to expand recruitment efforts this year, increasing the number of contacts for advertising the summer program. Again the course was approved by the Los Angeles Unified School District for salary point credit, and LAUSD advertised it on their web site of professional development opportunities. In addition to email announcements to various list-serves, we also sent personal letters to over 150 department science chairs, covering a large portion of the LA basin. For both years, the teachers represented a variety of academic backgrounds and classroom levels, including continuation schools and Advance Placement biology.

The 2007 program (5 Photos included) included lectures and lab work on topics including: genetics; plant physiology; the scientific process; current botanical research; growing Wisconsin Fast Plants and using them in the classroom; diffusion and osmosis; sexual and asexual reproduction; plant hormones; and plant morphology. The class even took a field trip to the Los Angeles Zoo to learn about plant/animal interactions and adaptations. Lectures and labs were lead and facilitated by Huntington staff with guest lectures from

- Dr. Elliot Meyerowitz, George W. Beadle Professor of Biology and Chair of the Division of Biology at the California Institute of Technology.
- Dr. Eric Mjolsness, Associate Professor, Department of Information and Computer Science at the University of California at Irvine
- Dr. Jose Luis Reichmann, Director, Gene Expression Center at Caltech
- Elaine Wong, Graduate student at the University of California at Irvine
- Sean Gordon, Graduate student at the California Institute of Technology

Our follow up workshops have provided additional labs and lectures on a variety of topics that help strengthen and expand the use of plants in the classroom. The workshops in the 2007-2008 series were:

- **October 27th, 2007: "Lesson Sharing and Discussions with Program Graduates."** Participants shared the lesson plans that they designed as part of the course with each other and received valuable input from their peers.
- **November 17th, 2007: "I'm Your Venus: Carnivorous Plants in the Classroom."** Ecology and evolution standards were addressed with an engaging look at the peculiar world of carnivorous plants. Participants experimented with (and took home) meat-eating flora, including the ever-famous Venus' fly trap.

- **February 9th, 2008: “Hormones in the Harvest.”** Dr. Deb Folsom of the Huntington and Pasadena City College gave a guest lecture about how people manipulate plant hormones so that we have “better” consumable goods. This fascinating talk ended with a trip to see the Camellia Festival, where there were beautiful and interesting examples of what can happen when these hormones are manipulated.
- **March 8th, 2008: “Composters Make It From The Ground-Up.”** Decomposers are an integral but often hidden part of the food web. In this workshop, participants looked closely (even microscopically) at the decomposition process and learned how to bring it into the classroom as a fascinating illustration of the carbon and nitrogen cycles.
- **April 26th, 2008: “Invasives”.** In this workshop, teachers studied the characteristics of invasive plants and did some mathematical modeling with UCI graduate student Elaine Wong to predict an invasive plant’s ability to spread.

While the dates of the 2008-2009 workshops have yet to be determined, they will follow the same topics and roughly the same distribution throughout the year as 2007-2008.

We are extremely pleased with the reactions from our participants. Comments such as “[*Grounding in Botany*] completely exceeded my expectations” and “I feel like I got great ideas for my classroom and learned a lot myself” were common in our evaluations, and we continued to hear praise for the course as the teachers were supported through workshops. At our most recent workshop, for example, one teacher took aside an instructor to let her know just how many lessons and activities from the course she has incorporated into her classroom already and how, most importantly, she now has the confidence to teach about plants where she hadn’t before. Some participants have even brought family members to attend follow-up workshops because they were so excited about the material. Another extremely important outcome of the *Grounding in Botany* course is the camaraderie and sharing of ideas and resources among participants. At each follow-up workshop, participants compare labs completed and activities planned, share successes and discuss challenges, trade lesson plans, and share stories about student achievements.

On our front-end and summative evaluation of participants to assess the success of the program, biology content scores raised an average of 27 percent after completion of the 2007 summer institute. A post-test at the end of the 2007-2008 academic year showed that teachers retained 90% of their summer content knowledge (over 8-months later). Additionally, teachers’ intent to make botanical sciences and botanical lab work a part of their classroom curriculum increases substantially, as does their level of confidence in teaching about plant biology. “I never knew I could learn so much hands-on valuable info for my class in such a short period... A class I will always remember and cherish” said one participant. Another added, “The course is very practical. If I had botany taught to me like this in undergrad, I’d be a botanist today.” These comments are backed by our year-end evaluation in which teachers reported a significant increase in the number of plant based labs they were using in their classroom (an average of eleven plant labs).

Not only do participants gain more content knowledge in botany, but evaluation has revealed that they also gain the skills to translate that knowledge to their students in meaningful ways. The 13 2007-2008 teachers and 14 2008-2009 teachers we worked with this year together will impact over 3000 students in this academic year alone—and evidence shows that the performance of those students will improve. For example, after all the high school science teachers in the Pasadena Unified School District (PUSD) attended Huntington workshops based on GIB materials, the scores of PUSD students (where 65% students are eligible for federal free-reduced lunch and 30% are English language learners) on the 2005–2006 California Standards Test in biology rose by 10 percent.

This June we had a proposal accepted for the National Meeting of The American Public Garden Association (APGA) where we gave a one day-workshop highlighting the *Grounding in Botany* program and disseminating several of the labs to Botanical Educators from around the country. Also, many of our labs have been posted on the *Grounding in Botany* webpage of the Huntington Garden's website (<http://www.huntington.org/Education/giblessons.html>) for increased dissemination potentials to all teachers.

For the 2008-2009 summer institute, we will offer a modified version of the *Grounding in Botany*. This version will utilize a cadre of teachers from previous years' who each bring 2 colleagues from their school to the program and develop the curriculum toward the level of school adoption. The teachers who have participated in the program will be co-teaching the material to their colleagues. We have also started talks with faculty from the Cal-State system to try to integrate the *Grounding in Botany* course into pre-service training for graduate students pursuing their Master's of Teaching in Science.









7. Dissemination

Journal Publications

“Antagonistic Regulation of PIN Phosphorylation by PP2A and PINOID Directs Auxin Flux”, M. Michniewicz, M. K. Zago, L. Abas, D. Weijers, A. Schweighofer, I. Meskiene, M. G. Heisler, C. Ohno, J. Zhang, F. Huang, R. Schwab, D. Weigel, E. M. Meyerowitz, C. Luschnig, R. Offringa, and J. Friml, *Cell* 130, 1-13, Sept 21 2007.

“An Exact Accelerated Stochastic Simulation Algorithm”, E. Mjolsness, D. Orendorff, P. Chatelain, P. Koumoutsakos, *submitted*.

“Mathematical Model of Auxin Distribution in the Plant Root”, V. A. Likhoshvai, N. A. Omel'yanchuk, V. V. Mironova, S. I. Fadeev, E. D. Mjolsness, and N. A. Kolchanov. *Russian Journal of Developmental Biology*, Vol. 38, No. 6, pp. 374–382, 2007.

“A Model Study of the Role of Proteins CLV1, CLV2, CLV3, and WUS in Regulation of the Structure of the Shoot Apical Meristem”, S. V. Nikolaev, A. V. Penenko, V. V. Lavreha, E. D. Mjolsness, and N. A. Kolchanov. *Russian Journal of Developmental Biology*, Vol. 38, No. 6, pp. 383–388, 2007.

“Towards a Calculus of Biomolecular Complexes at Equilibrium”, Eric Mjolsness. *Briefings in Bioinformatics*, 8(4):226-33 July 2007.

“On Cooperative Quasi-Equilibrium Models of Transcriptional Regulation”, Eric Mjolsness. *Journal of Bioinformatics and Computational Biology*, vol 5 no 2(b) pp 467-490, 2007.

Book Chapters

“Towards the Inference of Stochastic Biochemical Network and Parameterized Grammar Models”, Yosiphon, G. and E. Mjolsness. In N. Lawrence et al., eds., *Learning and Inference in Computational Systems Biology* (title with MIT Press), accepted 2008 for publication 2009.

Oral Presentations

Marcus Heisler, February 14th, 2008. Keystone meeting on Plant Hormones and Signaling. Auxin Transport Patterning and Primordium Development at the Shoot Apical Meristem.

E. Meyerowitz, September 18, 2007 University of Maryland, Symposium on Grand Challenges in 21st Century Bioscience

E. Meyerowitz, October 22, 2007 North Carolina Biotechnology Center, Research Triangle Park,

- E. Meyerowitz, November 9, 2007 Duke University, Computational Developmental Biology: How Mathematics, Computers and Genetics Combine to Explain Plant Development.
- E. Meyerowitz, November 28, 2007 University of Wisconsin, How the Shoot Apical Meristem Works: Dynamic Imaging, Genetics and Computational Models.
- E. Meyerowitz, January 25, 2007 Rockefeller University, Computational Morphodynamics: Live Imaging and Computational Modeling of Plant Stem Cells in the Shoot Apical Meristem.
- E. Meyerowitz, March 3, 2008 B.I.G. Lecture, University of Lausanne, Plant Stem Cells: Live Imaging and computational Models of the Arabidopsis Shoot Apical Meristem.
- E. Meyerowitz, March 6, 2008 Mendel Lecture, Academy of Science of the Czech Republic, Brno, Plant Stem Cells: Live Imaging and computational Models of the Arabidopsis Shoot Apical Meristem.
- E. Meyerowitz, May 20, 2008 U.C. Santa Barbara, Computational Morphodynamics: Live Imaging and Computational Modeling of Plant Stem Cell in the Shoot Apical Meristem.
- E. Mjolsness, “Computational Morphodynamics”, Computational Morphodynamics Workshop, Beckman Network Modeling Center (BNMC), Caltech, May 21 2008.
- E. Mjolsness, “Prospects for Computational Morphodynamics”, invited talk, CPIB Workshop on Auxin Transport, Center for Plant Integrative Biology, Nottingham, May 16 2008.
- E. Mjolsness, “Cellerator, Sigmoid, Cellzilla, and Plenum”, invited talk, CPIB Workshop on Auxin Transport, Center for Plant Integrative Biology, Nottingham, May 15 2008.
- E. Mjolsness, “Opportunities and challenges in cyberinfrastructure development”, invited talk, iPlant kickoff meeting, Cold Spring Harbor, April 8 2008.
- E. Mjolsness, “Computational Frameworks for Developmental Biology”, invited talk, UCI Developmental Biology Center retreat, March 17, 2008.
- E. Mjolsness, “Computational Frameworks for Phyllotaxis and Morphodynamics”, invited talk, Workshop on Morphogenesis, Kavli Institute for Theoretical Physics, March 3, 2008.
- E. Mjolsness, “New Mathematical Methods for Systems Biology”, Tutorial, International Society for Systems Biology (ICSB 2007), Long Beach California, 2:00 - 5:00 PM, Monday October 1, 2007.
- E. Mjolsness, “A Random Steady State model for the activity of Pyruvate Dehydrogenase”, invited talk, System Biology for Microbes at the 6-th Annual

International Conference on Computational Systems Bioinformatics (CSB 2007), Life Science Society, San Diego, August 2007.

E. Mjolsness, “Computational Support for Theory in Science”, invited discussion provocation, Caltech e-Science and Cyberinfrastructure Workshop, June 13, 2007.

Bruce Shapiro, Developmental Modeling of the Shoot Apical Meristem, Johan Radon Institute of Computational and Applied Mathematics, Special Semester on Quantitative Biology, Linz, Austria, Nov. 2007.

Guy Yosiphon, “Stochastic Multiscale Modeling Methods for Stem Cell Niches”, NIPS workshop on Machine Learning for Computational Biology, December 2007.

Poster presentations

“A receptor kinase is required for giant cell formation in *Arabidopsis* sepals”
Adrienne H. K. Roeder, Carolyn K. Ohno, and Elliot M. Meyerowitz, Poster presentation 18th International Conference on Arabidopsis Research. Beijing, China, 20-23 June 2007 (Roeder).

“Topological Index of a Model of p53 Dynamics Triggered by DNA Damage”, V. P. Golubyatnikov and E. Mjolsness, 6th International Conference on the Bioinformatics of Genome Regulation and Structure BGRS 2008.

“Finite Element Modeling of Mechanical Properties of Plant Cells in *Arabidopsis thaliana*”, Pawel Krupinski, Marcus Heisler, Patrick Hung, Elliot Meyerowitz, and Eric Mjolsness, Poster and Proceedings extended abstract, ICSB 2007: The Eighth International Conference on Systems Biology, Long Beach California, Oct 2-4 2007.

“1D Modeling of Auxin Distribution in Plant Roots”, Vitaly V. Likhoshvai, Victoria V. Mironova, Nadya A. Omelanchuk, Stanislav I. Fadeev, Nikolay A. Kolchanov, and Eric D. Mjolsness, Poster and Proceedings extended abstract, ICSB 2007: The Eighth International Conference on Systems Biology, Long Beach California, Oct 2-4 2007.

“Modeling of the Shoot Apical Meristem Structure Regulation Based on CLV1, CLV2, CLV3 and WUS Interactions”, Sergey Nikolaev, Alexey Penenko, Viktoriya Lavreha, Pavel Smal, Eric Mjolsness, and Nikolay Kolchanov Poster and Proceedings extended abstract, ICSB 2007: The Eighth International Conference on Systems Biology, Long Beach California, Oct 2-4 2007.

“Mathematica Platforms for Modeling in Systems Biology: Recent Developments in MathSBML and Cellerator”, Bruce E. Shapiro, James Lu, Michael Hucka, Eric D. Mjolsness, Poster and Proceedings extended abstract, ICSB 2007: The Eighth International Conference on Systems Biology, Long Beach California, Oct 2-4 2007.

“Integrating system for segmenting and tracking fluorescent objects on the image data of growing cell colonies”, Tigran Bacarian and Eric Mjolsness, Poster and Proceedings extended abstract, ICSB 2007: The Eighth International Conference on Systems Biology, Long Beach California, Oct 2-4 2007.

“High-accuracy R-leaping: Implementing and Exploring a Potentially Exact method for Accelerated Stochastic Simulation” D. Orendorff, P. Chatelain, P. Koumoutsakos, and E. Mjolsness, Poster and Proceedings extended abstract, ICSB 2007: The Eighth International Conference on Systems Biology, Long Beach California, Oct 2-4 2007.

“Dynamical Grammar Modeling of Cellular Proliferative Dynamics in the Olfactory Epithelium”, G. Yosiphon, K. K. Gokoffski, A. L. Calof, A. D. Lander, E. Mjolsness. Poster and Proceedings extended abstract, ICSB 2007: The Eighth International Conference on Systems Biology, Long Beach California, Oct 2-4 2007.

Press

Barbara Ellis, “Greening the Classroom”, Caltech News v 24 no. 4, 2007. Reports on Martha Kirouac’s Computable Plant outreach project at Huntington Botanical Gardens. <http://pr.caltech.edu/periodicals/CaltechNews/archive.html> .

Software

Recently updated versions of many Computable Plant project codes can be found on the project web site, www.computableplant.org → software.

In addition the Computable Plant PI’s have teamed up with others to propose a grand challenge project in Computational Morphodynamics to the new iPlant Collaborative, that could deliver tools incorporating knowledge and progress from the Computable Plant project to a much wider community of plant biologists. Successful proposers cannot expect to receive any funding as a result of their success, gaining instead just the right to advise iPlant on what problems to tackle and how. Preliminary success in this public service effort is recorded at <http://www.iplantcollaborative.org/component/content/article/49-public/113-grand-challenge-workshops-in-2008> .

Meetings

Through competitive proposals the PI’s have won the rights to hold two funded international followup meetings relating to Computational Morphodynamics: the iPlant Grand Challenge Workshop (see Software, above) in December 2008, and (with UCI’s Clare Yu) a future Kavli Institute for Theoretical Physics (KITP) short program in “Morphodynamics for Plants, Animals and Beyond” in Santa Barbara.